

Inverse orbital Hall effect induced terahertz emission enabled by a ferromagnet with quenched orbital moment in Fe/Pt/W trilayers

Chao Zhou^{1†}, Lei Hao^{1†}, Shaohua Zhang^{1†}, Yaxuan Jin¹, Xianguo Jiang¹, Ning Yang¹, Li Zheng¹, Hao Meng¹, Chao Lu¹, Wendeng Huang¹, Yizheng Wu^{2,3*}, Yan Zhou^{4*}, Jia Xu^{1*}

¹Department of Physics, School of Physics and Telecommunication Engineering, Shaanxi University of Technology, Hanzhong 723001, China

²Department of Physics and State Key Laboratory of Surface Physics, Fudan University, Shanghai 200433, China

³ Shanghai Research Center for Quantum Sciences, Shanghai 201315, China

⁴ Guangdong Basic Research Center of Excellence for Aggregate Science, School of Science and Engineering, The Chinese University of Hong Kong, Shenzhen, Shenzhen, Guangdong 518172, China

[†]These authors contributed equally to this work.

Abstract

The inverse orbital Hall effect (IOHE) has recently attracted considerable attention as an emerging mechanism for terahertz (THz) emission based on ultrafast angular-momentum-to-charge conversion. Most experimental studies have focused on materials with strong spin-orbit coupling or pronounced orbital character, where sizable orbital Hall responses are expected. Elemental ferromagnets such as Fe are generally regarded as quenched orbital sources and are not expected to exhibit orbital-dominated THz emission. Here, we report a pronounced enhancement of THz emission in Fe/Pt/W trilayer heterostructures, despite the absence of detectable orbital contributions in the corresponding Fe/Pt and Fe/W bilayers. Thickness-dependent measurements reveal long-distance signal persistence, systematic delay accumulation, and pronounced pulse broadening with increasing W thickness. These features are inconsistent with diffusive spin transport and indicate that orbital angular momentum transport in the W layer, converted into charge current via the IOHE, becomes a dominant channel for THz emission in the trilayer configuration. Our results demonstrate that strong IOHE can emerge in heterostructures incorporating a quenched orbital ferromagnet, providing an effective route to enhance spintronic THz emitters through orbital Hall physics.

1. Introduction

Spintronic terahertz (THz) emitters based on ultrafast angular momentum-to-charge conversion have emerged as a versatile platform for broadband THz generation, combining sub-picosecond temporal resolution, compact geometry, and compatibility with on-chip integration [1-3]. In conventional ferromagnet (FM)/heavy-metal (HM) heterostructures, femtosecond laser excitation generates nonequilibrium spin currents in the FM layer, which are converted into transverse charge currents via the inverse spin Hall effect (ISHE), giving rise to single-cycle THz emission [4-7]. This ISHE-based mechanism has been widely demonstrated in various FM/HM systems [8-11].

A fundamental limitation of ISHE-driven THz emitters, however, is the short spin diffusion length in typical heavy metals such as Pt and W [12, 13], which restricts efficient charge conversion to ultrathin layers. As a result, increasing the HM thickness leads to rapid signal attenuation due to spin relaxation and THz absorption. This constraint has stimulated growing interest in alternative transport channels that could enable long-range angular momentum propagation.

Recently, orbital angular momentum has been recognized as a promising complement to spin transport [14-19]. Both theoretical and experimental studies have shown that orbital currents generated via the orbital Hall effect (OHE) can propagate over much longer distances and be converted into charge currents through inverse orbital conversion mechanisms such as the inverse orbital Hall effect (IOHE) or inverse orbital Rashba-Edelstein effect (IOREE) [20-22]. These orbital-mediated processes have been linked to distinct THz emission signatures, including long-distance signal persistence, thickness-dependent delay accumulation, and pulse broadening [23-26].

Despite these advances, orbital-dominated THz emission has so far been demonstrated mainly in systems specifically engineered to support strong orbital responses [27, 28]. Recent studies have reported enhanced THz emission in CoPt/Pt/W heterostructures, where orbital angular momentum plays an important role [29]. In such systems, the ferromagnetic CoPt alloy itself acts as a strong intrinsic source of orbital

currents, and both Pt and W possess orbital Hall angles of the same sign, facilitating constructive orbital contributions. In contrast, elemental ferromagnets such as Fe are generally regarded as having their orbital moment quenched, and IOHE-related contributions are therefore expected to be negligible in Fe-based heterostructures [30]. Consistent with this expectation, Fe/Pt and Fe/W bilayers typically exhibit purely spin-current-dominated THz emission, with no clear signatures of long-range orbital angular momentum transport [31, 32].

In this work, we demonstrate that this expectation breaks down in Fe/Pt/W trilayers. Although both Fe/Pt and Fe/W bilayers are purely ISHE-dominated, the Fe/Pt/W trilayer exhibits a pronounced enhancement of THz emission accompanied by long-distance signal persistence, systematic delay accumulation, and pulse broadening. These features cannot be explained by diffusive spin transport alone. By systematically varying the Pt and W thicknesses, we demonstrate that orbital angular momentum transport in the W layer, converted into charge current via the IOHE, becomes a dominant channel for THz emission in Fe/Pt/W trilayers. Importantly, this strong orbital contribution emerges only in the trilayer configuration and is absent in the corresponding bilayers, despite the quenched orbital character of Fe. Our results establish a clear experimental route to activate orbital Hall physics in heterostructures based on elemental ferromagnets and highlight trilayer design as an effective strategy for enhancing spintronic THz emitters.

2. Experiments

Sample Fabrication:

A series of Fe/Pt/W heterostructures were fabricated on 1-mm-thick glass substrates using magnetron sputtering at room temperature. The heavy-metal layers of Pt and W were deposited by DC sputtering, while the Fe layer was grown by RF sputtering. The base pressure of the chamber was maintained below 3.5×10^{-5} Pa, and working pressure during deposition was approximately 0.2 Pa. The deposition rates

were calibrated to about 1 nm/min for Pt, and about 2 nm/min for Fe and W. The layer thickness was controlled by deposition time, ranging from 0 to 100 nm depending on the designed structure. All stacking sequences are described from bottom to top, with the first layer deposited directly onto the glass substrate. The thickness of the ferromagnetic Fe layer was fixed at 2 nm for all samples to ensure consistent angular momentum injection characteristics.

THz Emission Measurements: THz emission spectroscopy measurements were performed at room temperature in a dry air environment with relative humidity below 5%. A schematic diagram of the THz emission measurement setup is presented in Figure 1a. During measurements, samples were mounted in an electromagnet providing a 1000 Oe in-plane magnetic field along the x-axis, with the laser pulses incident normally from the substrate side. The laser pulses used in the experiments are linearly polarized, which are generated from a Ti:Sapphire laser oscillator (with a duration of \sim 80 fs, a center wavelength of 800 nm, and a repetition rate of 80 MHz). The pulse energy of the laser beam was kept below \sim 1.7 nJ to ensure that the emitted THz signal was linearly proportional to the laser intensity. The laser beam diameter was approximately 100 μ m. The emitted THz signal was detected using the electro-optic sampling technique with a 0.5 mm-thick electro-optic ZnTe(110) crystal.

3. Results and discussion

A. Emergent THz emission enhancement in Fe/Pt/W trilayers

Figure 1 presents a comparative overview of the THz emission characteristics of Fe/Pt and Fe/W bilayers and the Fe/Pt/W trilayer. As schematically illustrated in Figs. 1(a) and (b), both Fe/Pt and Fe/W bilayers are expected to exhibit THz emission dominated by ISHE. Owing to the opposite signs of the spin Hall angles of Pt ($\theta_{\text{SH},\text{Pt}} > 0$) and W ($\theta_{\text{SH},\text{W}} < 0$) [32-35], the two bilayers generate THz waveforms with opposite polarities, as confirmed by the time-domain signals measured from Fe(2 nm)/Pt(1.5 nm)

and Fe(2 nm)/W(0.75 nm) in Fig. 1(d). Notably, the THz amplitude of the Fe/Pt bilayer is significantly larger than that of Fe/W, which can be attributed to the larger effective spin Hall angle and thus, higher spin-to-charge conversion efficiency of Pt [36].

Based on these bilayer responses, a simple superposition model would predict that in a Fe/Pt/W trilayer the spin currents injected into Pt and W should generate THz emissions of opposite polarity, leading to partial cancellation and therefore a reduced overall THz output. Contrary to this expectation, the Fe/Pt/W trilayer exhibits a pronounced enhancement of the THz emission. As shown by the red curve in Fig. 1(d), the peak-to-peak amplitude ΔV of the trilayer far exceeds those of both Fe/Pt and Fe/W, and this non-additive enhancement is summarized in Fig. 1(e).

This anomalous enhancement immediately indicates that the THz response of the Fe/Pt/W trilayer cannot be explained by conventional spin-current-driven ISHE alone. Instead, the trilayer geometry enables an additional ultrafast angular momentum conversion pathway. As illustrated in Fig. 1(c), the Pt layer can enable conversion of spin angular momentum into orbital angular momentum, through its strong spin-orbit coupling [37]. The orbital currents might propagate over longer distances and be injected into the W layer, where they are converted into transverse charge currents via IOHE [29]. The constructive contribution of this orbital-to-charge conversion channel could then lead to the strongly enhanced THz emission observed in the Fe/Pt/W trilayer.

B. Spin-current-dominated THz emission in Fe/Pt and Fe/W bilayers

To establish a reliable baseline for spin-current-driven THz emission and to clarify whether orbital transport plays a role in Fe-based bilayers, systematic control experiments were performed on Fe/Pt and Fe/W bilayers with varying heavy-metal thicknesses. Figures 2(a) and 2(b) show representative time-domain THz waveforms of Fe/Pt and Fe/W bilayers at different thicknesses. In both systems, the THz amplitude decreases rapidly as the HM thickness increases.

The extracted peak-to-peak THz amplitudes ΔV are summarized in Fig. 2(c). For

$\text{Fe}(2 \text{ nm})/\text{Pt}(d_{\text{Pt}})$, ΔV reaches a maximum at $d_{\text{Pt}} \approx 2 \text{ nm}$ and then decreases sharply, approaching nearly zero at $d_{\text{Pt}} \geq 15 \text{ nm}$. A similar thickness-dependent attenuation is observed in $\text{Fe}(2 \text{ nm})/\text{W}(d_{\text{W}})$, although with opposite polarity due to the negative spin Hall angle of W. Such rapid decay is characteristic of ISHE-dominated charge conversion occurring within the initial few nanometers of the heavy-metal layer, together with enhanced THz absorption and electrical screening in thicker metallic films.

Despite the strong amplitude attenuation, the temporal position of the THz peak remains nearly unchanged across the entire thickness range for both bilayers. As shown in Fig. 2(d), the extracted delay time τ_D , obtained from the THz waveform (see details in Fig. S1 of the Supplementary Information [38]), varies only weakly with heavy-metal thickness and remains within a few femtoseconds of the reference value. This thickness-independent temporal behavior demonstrates that the THz pulse arrival time is governed by short-range diffusive spin transport rather than by long-range angular momentum propagation.

Further insight is provided by the THz pulse width analysis shown in Fig. 2(e). The pulse width Δt exhibits no systematic dependence on heavy-metal thickness for either Fe/Pt or Fe/W bilayers. Moreover, normalized time-domain waveforms at different thicknesses collapse onto a single curve (see Supplementary Fig. S2), indicating the absence of dispersive transport effects. These results unambiguously establish that THz emission in Fe/Pt and Fe/W bilayers is dominated by spin-current diffusion and ISHE-based charge conversion, with negligible contribution from orbital Hall transport [32]. This behavior is consistent with the quenched orbital moment of Fe, which is generally expected to generate only a small orbital angular momentum component [14].

C. Long-range angular momentum transport in Fe/Pt/W trilayers

In sharp contrast to the bilayer systems, Fe/Pt/W trilayers exhibit clear signatures of long-range angular momentum transport. Figure 3(a) shows representative time-

domain THz waveforms of Fe(2 nm)/Pt(2 nm)/W(d_W) as the W thickness is increased from 1 nm to 100 nm. Although the THz amplitude decreases monotonically with increasing d_W , a sizable THz signal remains detectable even at $d_W = 100$ nm. Such long-distance persistence of the THz signal is incompatible with spin diffusion, whose characteristic length in W is only a few nanometers [34].

The W thickness dependence of the signal amplitude ΔV for different Pt thicknesses is summarized in Fig. 3(b). Above the thickness of a few nanometers, while ΔV decreases with increasing d_W in all cases, the decay is significantly slower than that observed in Fe/W bilayers. To quantify this behavior, the dependence of ΔV on the W thickness in the regime of $d_W > 10$ nm is fitted using an exponential formula:

$$\Delta V(d_W) = \Delta V_0 \exp(-d_W/d_h) \quad (1)$$

where ΔV_0 is the THz signal amplitude and d_h is an effective decay length. As shown in Fig. 3(c), d_h exhibits a pronounced dependence on Pt thickness and reaches a maximum near $d_{Pt} \approx 2$ nm, indicating the slowest rate of decay.

The THz pulse width exhibits pronounced broadening with increasing W thickness when the Pt thickness is fixed at 2 nm, as shown in Fig. 3(d). In contrast, for Pt thicknesses of 1 nm and 3 nm the pulse width shows much weaker dependence on W thickness. Temporal analysis provides direct evidence for propagating angular momentum. As shown in Fig. 3(e), the delay time τ_D increases approximately linearly with W thickness for all investigated Pt thicknesses. Assuming a ballistic transport regime, the transport velocity can be found as the inverse of slope, as in Fig. 3(f). The linear fits yield effective propagation velocities on the order of 0.3~0.6 nm/fs for Fe/Pt/W trilayer, and ~ 1.0 nm/fs for Fe/W bilayer. The high velocity observed in Fe/W agrees with the properties of ultrafast spin currents [39]. The significantly slower transport in Fe/Pt/W is inconsistent with spin diffusion, and suggested orbital angular momentum propagation in the W layer [40]. The slowest velocity occurred when Pt is 2 nm, suggesting that the contribution from IOHE might be strongest in this case. The coexistence of long-distance propagation, thickness-dependent delay accumulation,

and pulse broadening provides compelling evidence that orbital Hall transport and IOHE-based charge conversion dominate the THz emission process in Fe/Pt/W trilayers.

D. Thickness-matched ISHE-IOHE cooperative enhancement mechanism

The thickness dependence of the THz enhancement reveals that orbital transport alone is not sufficient to maximize the THz output. Figure 4(a) depicts the mechanism for THz emission in Fe/Pt/W: upon laser excitation, a strong spin current j_S and a quenched orbital current j_L are both injected into Pt. Through the ISHE in Pt, j_S is converted into a charge current j_C , and generates THz emission. On the other hand, the strong spin orbit coupling in Pt also converts j_S into j_L [29, 37]. The orbital current from the conversion in Pt can be much stronger than that from Fe directly. In total, j_L gets converted into j_C via the IOHE in W, also creating THz emission, the charge currents generated by the ISHE in Pt and the IOHE in W possess the same polarity, allowing the spin- and orbital-originated THz signals to coherently interfere and jointly modulate the overall THz emission amplitude. To learn about the cooperation of THz emission from both mechanisms, we investigated the evolution of THz emission when the thickness of W is very thin.

Figure 4(b) shows the evolution of the THz signal from Fe(2 nm)/Pt(d_{Pt})/W(d_W) when the W thickness d_W is fixed at 0.75 nm. As d_{Pt} increases from 0 to 2 nm, the THz amplitude increases monotonically, indicating a progressively enhanced emission. When the d_{Pt} exceeds 2 nm, however, the THz signal gradually decreases. In contrast, as shown in Fig. 4(c), when the d_{Pt} is fixed at 2 nm, the THz signal exhibits a different dependence on the d_W , reaching its maximum at $d_W \approx 0.5$ nm. This distinct behavior highlights that the optimal enhancement condition depends sensitively on the thickness matching between Pt and W layers.

As shown in Fig. 4(d), when the thickness of W is fixed at 0.75 nm and 2 nm, ΔV initially always increases with d_{Pt} , and a maximum value is reached when d_{Pt} is about 2 nm. To better describe the enhancement from the cooperation of ISHE and IOHE, we

have defined an enhancement factor η :

$$\eta(d_{\text{Pt}}, d_W) = \frac{\Delta V_{\text{Fe}/\text{Pt}(d_{\text{Pt}})/\text{W}(d_W)}}{\Delta V_{\text{Fe}/\text{Pt}(d_{\text{Pt}})} + \Delta V_{\text{Fe}/\text{W}(d_W)}} \quad (2)$$

The trends for η are summarized in Fig. 4(e). It is clear that when d_W is 0.75 nm, there is a wide range of d_{Pt} (0.5~2.5 nm) that enables enhancement of THz emission, with enhancement factor $\eta > 1$. When d_W is increased to 2 nm, the value of η becomes generally smaller than 1, with only one exception at around $d_{\text{Pt}} = 1\text{--}1.5$ nm. Those results suggest $d_{\text{Pt}} \sim 1.5$ nm as the condition to achieve optimal enhancement.

On the other hand, the trends in ΔV as a function of d_W are shown in Fig. 4(f). It is clear that as d_{Pt} increases, the corresponding d_W of peak gradually shifts to the left until it becomes zero, leading to monotonically decreasing signal when Pt thickness is 3 nm. The trends of η for the corresponding samples are summarized in Fig. 4(g), revealing its complex dependence on d_W .

When d_{Pt} is 1 nm, η first increases with d_W , reaching a peak at 2 nm, and then decreases. At around $d_W \sim 4$ nm, η passes the threshold of 1, suggesting a conversion from the enhancement region to a suppression one. As d_{Pt} increases to 2 nm, the peak for η occurred at $d_W \sim 0.5$ nm.

This behavior reflects a thickness-matched cooperative mechanism between ISHE and IOHE. For ultrathin Pt layers, partial orbital injection into W can already occur, giving rise to detectable IOHE-related signatures. However, the Pt layer might not be fully continuous and the ISHE-induced charge current is spatially inhomogeneous, limiting the cooperative enhancement. When the Pt thickness increases to approximately 2 nm, the spin current injected from Fe is more efficiently converted into a transverse charge current via ISHE in Pt, while simultaneously generating a strong orbital polarization through spin-orbit coupling. The resulting orbital current is subsequently injected into W and converted into an additional charge current via IOHE. The temporal and spatial overlap between the prompt ISHE response in Pt and the delayed IOHE contribution in W leads to the maximum THz enhancement.

For Pt layers thicker than 3nm, orbital transport and IOHE conversion in W remain present, as evidenced by the continued delay accumulation and pulse broadening [15]. However, the spin current injected from Fe is largely relaxed within the Pt layer before reaching the Pt/W interface, resulting in a reduced ISHE contribution. Consequently, the cooperative ISHE-IOHE mechanism becomes inefficient, and no further enhancement of the THz amplitude is observed despite the persistence of orbital transport.

In addition, reversing the stacking order of Pt and W would disable both the emission enhancement and the long-distance transport (See Supplementary Figure S5). That highlights the importance for the strong spin-to-orbital conversion in Pt, along with the strong IOHE in W in promoting such effects. Overall, these results demonstrate that the enhanced THz emission in Fe/Pt/W trilayers originates from a thickness-matched ISHE-IOHE cooperative mechanism, in which the Pt/W combination effectively amplifies the otherwise quenched orbital character of Fe. This work highlights the importance of interface engineering and thickness optimization in activating orbital angular momentum transport and provides a practical strategy for designing high-performance spin-orbitronic THz emitters.

4. Conclusion

In conclusion, we have demonstrated a pronounced and non-additive enhancement of THz emission in Fe/Pt/W trilayers that cannot be explained by conventional ISHE alone. Through systematic thickness-dependent and stacking-sequence-dependent investigations, we establish that Fe/Pt and Fe/W bilayers serve as clean spin-dominated reference systems, consistent with quenched orbital character of Fe. In these bilayers, THz emission is governed by short-range spin diffusion and ISHE-based charge conversion, with no detectable signatures of orbital Hall transport.

In sharp contrast, the Fe/Pt/W trilayer exhibits clear evidence of long-range angular momentum transport, including systematic delay accumulation, pulse

broadening, and finite THz signals persisting over tens of nanometers in W. These features unambiguously indicate the activation of orbital angular momentum transport and IOHE-based charge conversion. Crucially, the observed THz enhancement arises from a thickness-matched cooperative mechanism between ISHE in Pt and IOHE in W. When the Pt thickness is optimized (~ 2 nm), spin-to-charge conversion in Pt and orbital-to-charge conversion in W act constructively in both space and time, leading to maximal THz emission. For thinner or thicker Pt layers, although orbital transport and IOHE signatures may still exist, the cooperative enhancement is suppressed due to incomplete film continuity or excessive spin relaxation.

Our results establish ISHE-IOHE cooperation as a powerful and tunable route to enhance ultrafast THz emission, and demonstrate that orbital angular momentum, though quenched in conventional ferromagnets, can be effectively activated and amplified by interface engineering and thickness optimization. Beyond THz emitters, our trilayer strategy suggests a viable pathway to harness orbital degrees of freedom using standard ferromagnetic materials, opening opportunities for orbital-assisted information storage and logic functionalities in ultrafast spin-orbitronic devices.

Acknowledgements:

This work was supported by the National Natural Science Foundation of China (Grant No. 12204295 and 12204296), the Open Research Project of State Key Laboratory of Surface Physics from Fudan University (Grant No. KF2022_17), the Youth Science and Technology Star Program of Shaanxi Province (2025ZC-KJXX-15), the Young Talent Fund of Association for Science and Technology in Shaanxi (20250512), the Youth Project in Sanqin Talent Introduction Program, and the Shaanxi Province Outstanding Young Talent Support Program for Universities and Young Hanjiang Scholar of Shaanxi University of Technology, and Shaanxi University of Technology (Grants No. SLGRCQD044 and SLGRCQD046). The Innovation Fund of

Shaanxi University of Technology (Grant No. SLGYCX2514 and SLGYCX2511). Yizheng Wu acknowledges the support from the National Key Research and Development Program of China (Grant No. 2024YFA1408501), the National Natural Science Foundation of China (Grant No.11974079, 12274083, 1222100), the Shanghai Municipal Science and Technology Major Project (Grant No. 2019SHZDZX01), and the Shanghai Municipal Science and Technology Basic Research Project (Grant No. 22JC1400200). Hao Meng acknowledges the support from the National Natural Science Foundation of China (Grant No.12174238). Y. Z. acknowledges support by the Shenzhen Fundamental Research Fund (Grant No. JCYJ20210324120213037), and the National Natural Science Foundation of China (12374123), Guangdong Basic Research Center of Excellence for Aggregate Science, and the 2023 SZSTI stable support scheme.

Reference

- [1] T. Kampfrath, M. Battiato, P. Maldonado, G. Eilers, J. Nötzold, S. Mährlein, V. Zbarsky, F. Freimuth, Y. Mokrousov, S. Blügel, M. Wolf, I. Radu, P.M. Oppeneer, M. Münzenberg, Terahertz spin current pulses controlled by magnetic heterostructures, *Nature Nanotechnology*, 8 (2013) 256-260.
- [2] T. Seifert, S. Jaiswal, U. Martens, J. Hannegan, L. Braun, P. Maldonado, F. Freimuth, A. Kronenberg, J. Henrizi, I. Radu, E. Beaurepaire, Y. Mokrousov, P.M. Oppeneer, M. Jourdan, G. Jakob, D. Turchinovich, L.M. Hayden, M. Wolf, M. Münzenberg, M. Kläui, T. Kampfrath, Efficient metallic spintronic emitters of ultrabroadband terahertz radiation, *Nature Photonics*, 10 (2016) 483-488.
- [3] T.S. Seifert, L. Cheng, Z. Wei, T. Kampfrath, J. Qi, Spintronic sources of ultrashort terahertz electromagnetic pulses, *Applied Physics Letters*, 120 (2022) 0080357.
- [4] Y. Wu, M. Elyasi, X. Qiu, M. Chen, Y. Liu, L. Ke, H. Yang, High-Performance THz Emitters Based on Ferromagnetic/Nonmagnetic Heterostructures, *Advanced Materials*, 29 (2017) 1603031.
- [5] S. Kumar, S. Kumar, Large interfacial contribution to ultrafast THz emission by inverse spin Hall effect in CoFeB/Ta heterostructure, *iScience*, 25 (2022) 104718.
- [6] E.T. Papaioannou, L. Scheuer, G. Torosyan, G.P. Dimitrakopoulos, S. Kret, A.D. Crisan, O. Crisan, R. Beigang, T. Kehagias, Enhanced THz Emission From Ultrathin Ta/Fe/Pt Spintronic Trilayers, *Advanced Optical Materials*, 13 (2025) e00874.
- [7] I. Ilyakov, A. Brataas, T.V.A.G. de Oliveira, A. Ponomaryov, J.-C. Deinert, O. Hellwig, J. Faßbender, J. Lindner, R. Salikhov, S. Kovalev, Efficient ultrafast field-driven spin current generation for spintronic terahertz frequency conversion, *Nature Communications*, 14 (2023) 7010.
- [8] H. Cheng, Y. Wang, H. He, Q. Huang, Y. Lu, Efficient and temperature-independent terahertz emission from CoFeB/NiCu heterostructures, *Physical Review B*, 105 (2022) 155141.
- [9] T.J. Huisman, R.V. Mikhaylovskiy, J.D. Costa, F. Freimuth, E. Paz, J. Ventura, P.P. Freitas, S. Blügel, Y. Mokrousov, T. Rasing, A.V. Kimel, Femtosecond control of electric currents in metallic ferromagnetic heterostructures, *Nature Nanotechnology*, 11 (2016) 455-458.
- [10] J. Xu, S. Zhang, X. Jiang, Y. Jin, L. Hao, M. Jing, X. Cao, T. He, H. Meng, M. He, Y. Wu, W. Huang, Y. Zhou, C. Zhou, Spin current direction dependent terahertz emission induced by directional interfacial alloying in Co/Al/Pt trilayers, *Physical Review B*, 112 (2025) 104446.
- [11] G. Li, R.V. Mikhaylovskiy, K.A. Grishunin, J.D. Costa, T. Rasing, A.V. Kimel, Laser induced THz emission from femtosecond photocurrents in Co/ZnO/Pt and Co/Cu/Pt multilayers, *Journal of Physics D: Applied Physics*, 51 (2018) 1361-6463.
- [12] K. Roy, Estimating the spin diffusion length and the spin Hall angle from spin pumping induced inverse spin Hall voltages, *Physical Review B*, 96 (2017) 174432.
- [13] E. Sagasta, Y. Omori, M. Isasa, M. Gradhand, L.E. Hueso, Y. Niimi, Y. Otani, F. Casanova, Tuning the spin Hall effect of Pt from the moderately dirty to the superclean regime, *Physical Review B*, 94 (2016) 060412.
- [14] S. Kumar, S. Kumar, Ultrafast terahertz spin and orbital transport in magnetic/nonmagnetic multilayer heterostructures and a perspective, *Journal of Applied Physics*, 134 (2023) 170901.
- [15] S.S. Mishra, J. Lourembam, D.J.X. Lin, R. Singh, Active ballistic orbital transport in Ni/Pt heterostructure, *Nature Communications*, 15 (2024) 4568.
- [16] Y.-G. Choi, D. Jo, K.-H. Ko, D. Go, K.-H. Kim, H.G. Park, C. Kim, B.-C. Min, G.-M. Choi, H.-W.

Lee, Observation of the orbital Hall effect in a light metal Ti, *Nature*, 619 (2023) 52-56.

[17] D. Lee, D. Go, H.-J. Park, W. Jeong, H.-W. Ko, D. Yun, D. Jo, S. Lee, G. Go, J.H. Oh, K.-J. Kim, B.-G. Park, B.-C. Min, H.C. Koo, H.-W. Lee, O. Lee, K.-J. Lee, Orbital torque in magnetic bilayers, *Nature Communications*, 12 (2021) 6710.

[18] E. Santos, U. Borges, J.L. Costa, E.L.T. França, J.B.S. Mendes, A. Azevedo, Anomalous inverse spin and orbital Hall effects in Fe films with strong uniaxial anisotropy, *Physical Review Applied*, 10 (2025) 3449.

[19] P. Wang, F. Chen, Y. Yang, S. Hu, Y. Li, W. Wang, D. Zhang, Y. Jiang, Orbitronics: Mechanisms, Materials and Devices, *Advanced Electronic Materials*, 11 (2025) 2400554.

[20] R. Xu, X. Ning, H. Cheng, Y. Yao, Z. Ren, S. Liu, M. Dai, Y. Xu, S. Li, A. Du, X. Wu, F. Hu, B. Shen, J. Sun, H. Zhang, W. Zhao, Terahertz generation via the inverse orbital Rashba-Edelstein effect at the Ni/CuO_x interface, *Physical Review Research*, 7 (2025) L012042.

[21] C. Zhou, Y.P. Liu, Z. Wang, S.J. Ma, M.W. Jia, R.Q. Wu, L. Zhou, W. Zhang, M.K. Liu, Y.Z. Wu, J. Qi, Broadband Terahertz Generation via the Interface Inverse Rashba-Edelstein Effect, *Physical Review Letters*, 121 (2018) 086801.

[22] W. Li, Y. Wang, H. Cheng, J. Huang, B. Xiong, J. Huang, Q. Huang, Z. Cui, Z. Fu, Y. Lu, Significant orbit-to-charge conversion in CoFeB/Pt/SrIrO₃ trilayer by terahertz emission spectroscopy, *Applied Physics Letters*, 126 (2025) 062404.

[23] C. Guo, S. Yin, J. Yang, Y. Ren, P. Ji, Y. Zhang, H. Yan, J. Zhang, B. Cui, Y. Zuo, L. Ding, L. Xi, Ferromagnetic Ni enhances terahertz emission through the inverse orbital Hall effect in Ni/Ti bilayers, *Physical Review Applied*, 24 (2025) 024009.

[24] H. Xu, Y. Yang, Z. Jin, P. Wang, Z. Feng, T. Wang, W. Yue, C. Chen, F. Chen, Y. Zhu, Y. Peng, Z. Delin, Y. Jiang, S. Zhuang, Generation and manipulation of light-induced orbital transport in Co/Zr/Al₂O₃ heterostructure probed with ultrafast terahertz emission, *Communications Physics*, 8 (2025) 115.

[25] A. Bose, F. Kammerbauer, R. Gupta, D. Go, Y. Mokrousov, G. Jakob, M. Kläui, Detection of long-range orbital-Hall torques, *Physical Review B*, 107 (2023) 134423.

[26] H. Hayashi, D. Jo, D. Go, T. Gao, S. Haku, Y. Mokrousov, H.-W. Lee, K. Ando, Observation of long-range orbital transport and giant orbital torque, *Communications Physics*, 6 (2023) 32.

[27] T. Tanaka, H. Kontani, M. Naito, T. Naito, D.S. Hirashima, K. Yamada, J. Inoue, Intrinsic spin Hall effect and orbital Hall effect in 4d and 5d transition metals, *Physical Review B*, 77 (2008) 165117.

[28] G. Sala, P. Gambardella, Giant orbital Hall effect and orbital-to-spin conversion in 3d, 5d, and 4f metallic heterostructures, *Physical Review Research*, 4 (2022) 033037.

[29] Y. Zou, Y. Song, Z. Li, J. Zhang, H. Dai, X. Ma, Q. Jin, Z. Zhang, Enhanced Terahertz Emission via Synergistic Spin-Orbit Conversion in CoPt/Pt/W Multilayers, *Advanced Functional Materials*, 10 (2025) 202515949.

[30] D. Go, D. Jo, C. Kim, H.-W. Lee, Intrinsic Spin and Orbital Hall Effects from Orbital Texture, *Physical Review Letters*, 121 (2018) 086602.

[31] J.C. Rojas-Sánchez, A. Fert, Compared Efficiencies of Conversions between Charge and Spin Current by Spin-Orbit Interactions in Two- and Three-Dimensional Systems, *Physical Review Applied*, 11 (2019) 054049.

[32] T. Guan, J. Liu, W. Qin, Y. Cui, S. Wang, Y. Wu, Z. Tao, Evidence of Ultrashort Orbital Transport in

Heavy Metals Revealed by Terahertz Emission Spectroscopy, Arxiv, 2504 (2025) 15553.

[33] L. Liu, T. Moriyama, D.C. Ralph, R.A. Buhrman, Spin-Torque Ferromagnetic Resonance Induced by the Spin Hall Effect, *Physical Review Letters*, 106 (2011) 036601.

[34] C.-F. Pai, L. Liu, Y. Li, H.W. Tseng, D.C. Ralph, R.A. Buhrman, Spin transfer torque devices utilizing the giant spin Hall effect of tungsten, *Applied Physics Letters*, 101 (2012) 122404.

[35] J. Sinova, S.O. Valenzuela, J. Wunderlich, C.H. Back, T. Jungwirth, Spin Hall effects, *Reviews of Modern Physics*, 87 (2015) 1213-1260.

[36] D. Yang, J. Liang, C. Zhou, L. Sun, R. Zheng, S. Luo, Y. Wu, J. Qi, Powerful and Tunable THz Emitters Based on the Fe/Pt Magnetic Heterostructure, *Advanced Optical Materials*, 4 (2016) 1944-1949.

[37] R. Xu, H. Zhang, Y. Jiang, H. Cheng, Y. Xie, Y. Yao, D. Xiong, Z. Zhu, X. Ning, R. Chen, Y. Huang, S. Xu, J. Cai, Y. Xu, T. Liu, W. Zhao, Giant orbit-to-charge conversion induced via the inverse orbital Hall effect, Arxiv, 2308 (2023) 144.

[38] B.Y. Shahriar, A.Y. Elezzabi, Orbitronic terahertz emission from Mo-based nanolayers via the inverse orbital Hall and Rashba–Edelstein effects, *Applied Physics Letters*, 127 (2025) 0294721.

[39] J. Jechumtál, R. Rouzegar, O. Gueckstock, C. Denker, W. Hoppe, Q. Remy, T.S. Seifert, P. Kubaščík, G. Woltersdorf, P.W. Brouwer, Accessing ultrafast spin-transport dynamics in copper using broadband terahertz spectroscopy, *Physical Review Letters*, 132 (2024) 226703.

[40] T.S. Seifert, D. Go, H. Hayashi, R. Rouzegar, F. Freimuth, K. Ando, Y. Mokrousov, T. Kampfrath, Time-domain observation of ballistic orbital-angular-momentum currents with giant relaxation length in tungsten, *Nature Nanotechnology*, 18 (2023) 1132-1138.

Figures:

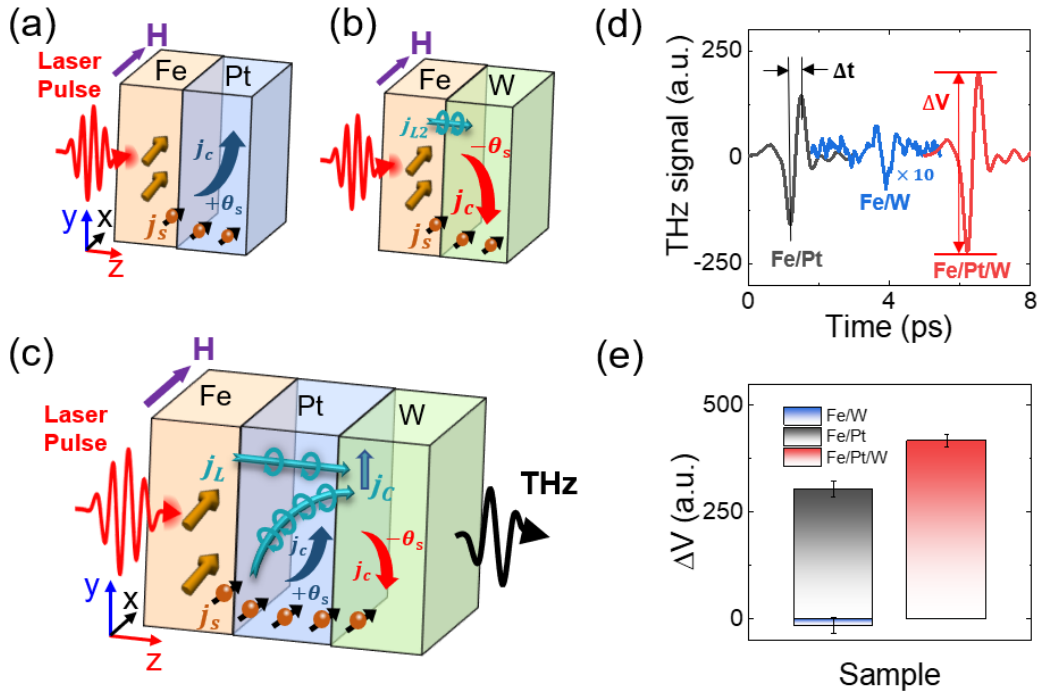


Figure 1 (a)-(c) Schematic illustrations of (a) Fe/Pt, (b) Fe/W, and (c) Fe/Pt/W bilayers under femtosecond laser excitation. (d) Representative time-domain THz waveforms emitted from Fe/Pt, Fe/W, and Fe/Pt/W samples, highlighting the enhanced peak-to-peak amplitude ΔV in the trilayer. The curves are shifted horizontally for clarity. (e) Comparison of the extracted ΔV for different sample structures in (d).

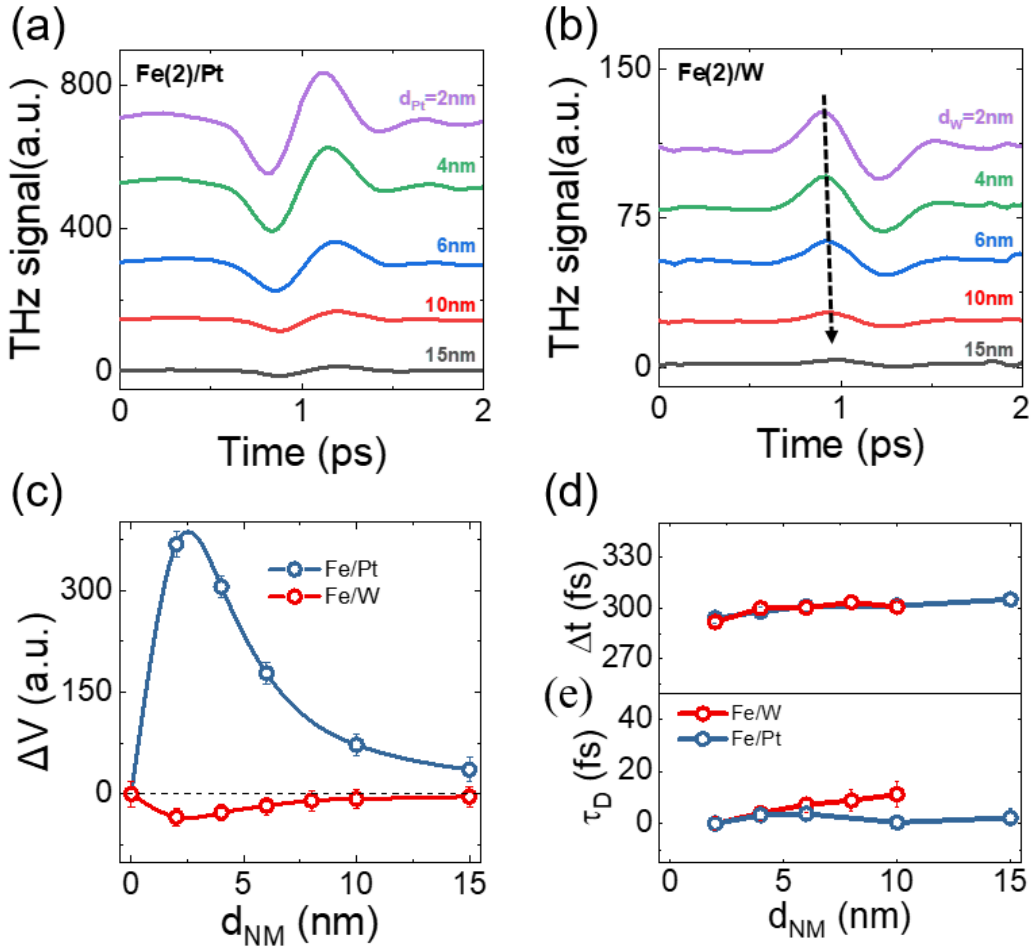


Figure 2 (a)-(b) Time-domain THz waveforms emitted from Fe(2 nm)/Pt(d_{Pt}) and Fe(2 nm)/W(d_{W}) bilayers with different nonmagnetic layer thicknesses, respectively. (c) Extracted peak-to-peak THz amplitudes ΔV as a function of nonmagnetic layer thickness d_{NM} for Fe/Pt and Fe/W bilayers. (d) THz pulse width Δt as a function of d_{NM} for Fe/Pt and Fe/W bilayers. (e) Extracted delay time τ_D of the THz peak as a function of d_{NM} for Fe/Pt and Fe/W bilayers.

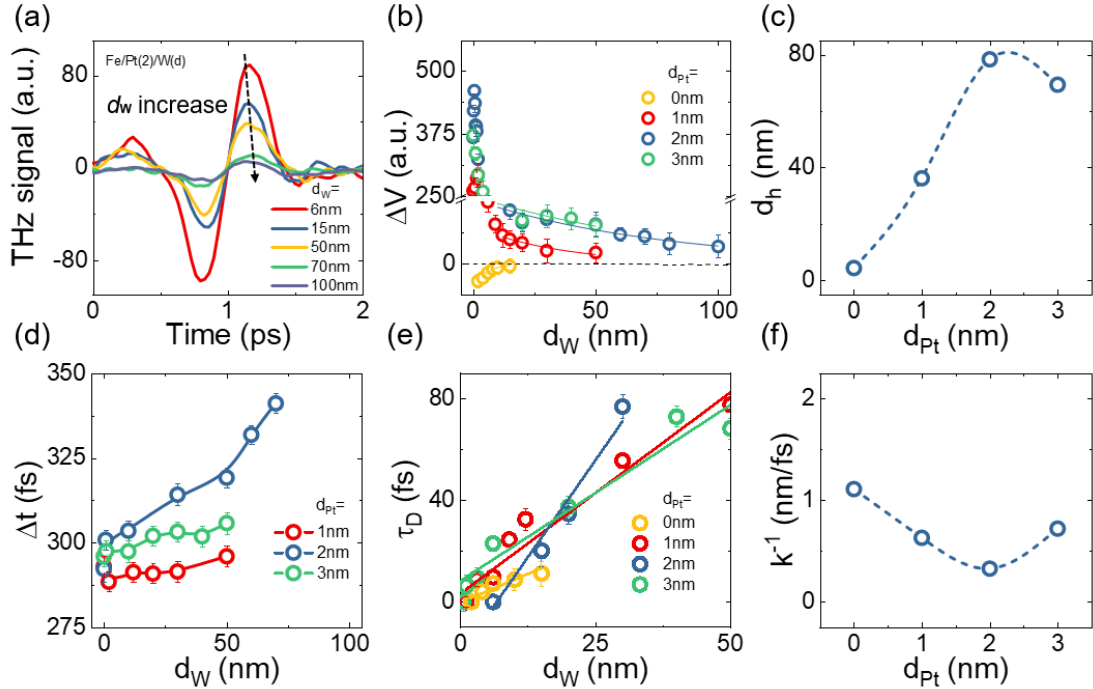


Figure 3 (a) Time-domain THz waveforms of Fe(2 nm)/Pt(2 nm)/W(d_W) trilayers with varying W thicknesses. (b) Extracted peak-to-peak THz amplitudes ΔV as a function of W thickness d_W for different Pt thicknesses d_{Pt} . The solid lines represent fitted curves with an exponential formula. (c) Extracted decay length d_h of the THz signal as a function of d_{Pt} . The dotted curve are guides to the eye. (d) THz pulse width Δt as a function of d_W for different d_{Pt} . The solid curve are guides to the eye. (e) Delay time τ_D of the THz peak as a function of d_W for different d_{Pt} , obtained from Hilbert transformation. (f) Transport velocity k^{-1} extracted from the linear fitting of τ_D versus d_W as a function of d_{Pt} . The dotted curve are guides to the eye.

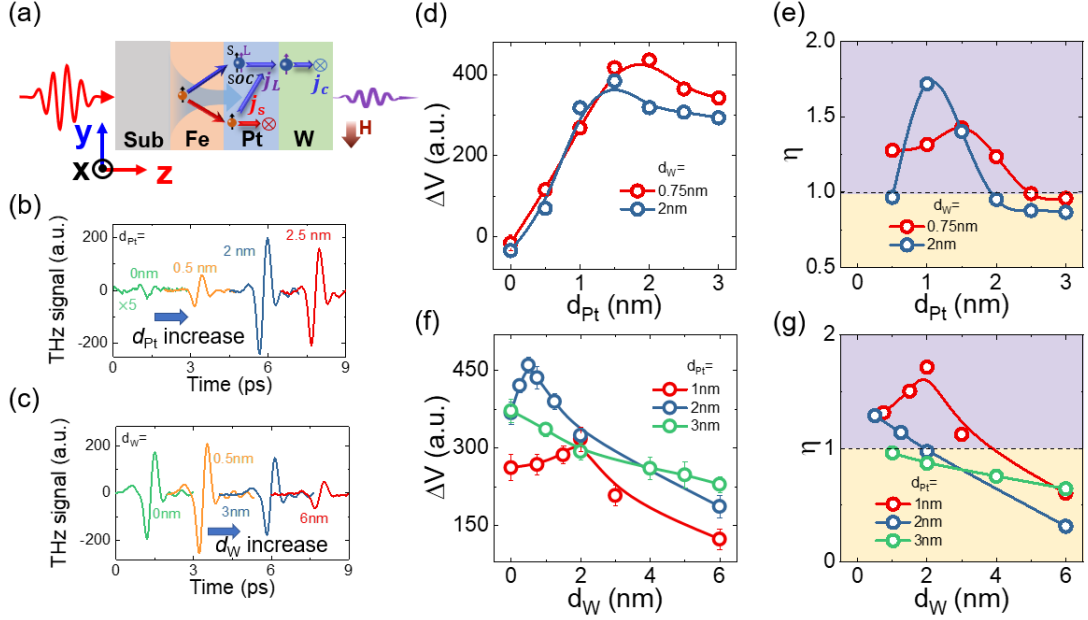


Figure 4 (a) Schematic illustration of the Fe/Pt/W trilayer under femtosecond laser excitation. (b)-(c) Time-domain THz waveforms of (b) Fe/Pt(d_{Pt})/W(0.75 nm) with varying Pt thicknesses d_{Pt} , and (c) Fe/Pt(2 nm)/W(d_W) with varying W thicknesses d_W . The curves are shifted horizontally for clarity. (d) Extracted peak-to-peak THz amplitudes ΔV as a function of d_{Pt} for different W thicknesses. (e) Enhancement factor η as a function of d_{Pt} for different W thicknesses. (f) Extracted peak-to-peak THz amplitudes ΔV as a function of d_W for different Pt thicknesses. (g) Enhancement factor η as a function of d_W for different Pt thicknesses.